SEUSS and *AINTEGUMENTA* Mediate Patterning and Ovule Initiation during Gynoecium Medial Domain Development[1][W][OA]

Sridevi Azhakanandam[2], Staci Nole-Wilson[2], Fang Bao, and Robert G. Franks*

Department of Genetics, North Carolina State University, Raleigh, North Carolina 27695

The Arabidopsis (*Arabidopsis thaliana*) gynoecium, the female floral reproductive structure, requires the action of genes that specify positional identities during its development to generate an organ competent for seed development and dispersal. Early in gynoecial development, patterning events divide the primordium into distinct domains that will give rise to specific tissues and organs. The medial domain of the gynoecium gives rise to the ovules, and several other structures critical for reproductive competence. Here we report a synergistic genetic interaction between *seuss* and *aintegumenta* mutants resulting in a complete loss of ovule initiation and a reduction of the structures derived from the medial domain. We show that patterning events are disrupted early in the development of the *seuss aintegumenta* gynoecia and we identify *PHABULOSA* (*PHB*), *REVOLUTA*, and *CRABS CLAW* (*CRC*) as potential downstream targets of *SEUSS* (*SEU*) and *AINTEGUMENTA* (*ANT*) regulation. Our genetic data suggest that *SEU* additionally functions in pathways that are partially redundant and parallel to *PHB*, *CRC*, and *ANT*. Thus, *SEU* and *ANT* are part of a complex and robust molecular system that coordinates patterning cues and cellular proliferation along the three positional axes of the developing gynoecium.

During organ development, positional identity information must be coordinated with cellular proliferation to achieve proper organ shape and function. In the Arabidopsis (*Arabidopsis thaliana*) gynoecium, the female reproductive floral structure, early patterning events divide the gynoecial primordium into distinct zones that distinguish adaxial (inner) versus abaxial (outer), medial versus lateral, and apical versus basal domains (Sessions and Zambryski, 1995; Sessions et al., 1997; Bowman et al., 1999; Ferrandiz et al., 1999; Sessions, 1999; Alvarez and Smyth, 2002). Subsequently, patterns of coordinated cell division and differentiation generate the mature structures that comprise the gynoecium. The Arabidopsis gynoecium is composed of two carpel organs that arise congenitally fused along their margins. The fused margins of the carpels comprise the medial domain of the gynoecium (Fig. 1). A meristematic ridge of tissue, termed the medial ridge (mr in the image), develops along the adaxial (inner) portion of the medial domain. Although clonal analysis data are not available, the patterns of gene expression and cell division, as well as genetic data, strongly suggest that the medial ridge generates the placenta, ovules, septum, and associated transmitting tract, as well as portions of the style and stigma; all of which are critical structures for reproductive competence (Bowman et al., 1999).

Many mutations that affect the development of the medial ridge-derived structures have been identified (Bowman et al., 1999; Ferrandiz et al., 1999; Sessions, 1999; Alvarez and Smyth, 2002; Balanza et al., 2006). However, many of these genes share functional redundancy, and more severe alterations of medial ridge development have been reported in a variety of double mutants. For example, *LEUNIG* (*LUG*) and *AINTEGUMENTA* (*ANT*) share an important and partially redundant function during the development of the gynoecial medial domain (Liu et al., 2000). The *lug* and *ant* single mutants display relatively mild disruptions of the medial domain (Liu and Meyerowitz, 1995; Elliott et al., 1996; Klucher et al., 1996). However, *lug ant* double-mutant gynoecia lack nearly all of the medial domain and its derived tissues: septum, stigma, ovules, and style (Liu et al., 2000).

ANT encodes a sequence-specific DNA-binding protein expressed early during organ development that functions in organ initiation and potentiates cellular divisions during organ development (Elliott et al., 1996; Klucher et al., 1996; Mizukami and Fischer, 2000; Nole-Wilson and Krizek, 2000). *LUG* encodes a transcriptional coregulator with sequence similarity to two protein families: the Tup1/Groucho and Ssdp/Chip

[1] This work was supported by the National Research Initiative of the U.S. Department of Agriculture Cooperative State Research, Education, and Extension Service (grant no. 2006–03378 to S.N.W.), the National Science Foundation (grant no. IOB–0416759 to R.G.F.), and the U.S. Department of Agriculture Agricultural Research Service (NC06759).

[2] These authors contributed equally to the article.

* Corresponding author; e-mail rgfranks@ncsu.edu.

The author responsible for distribution of materials integral to the findings presented in this article in accordance with the policy described in the Instructions for Authors (www.plantphysiol.org) is: Robert G. Franks (rgfranks@ncsu.edu).

[W] The online version of this article contains Web-only data.

[OA] Open Access articles can be viewed online without a subscription.

www.plantphysiol.org/cgi/doi/10.1104/pp.107.114751

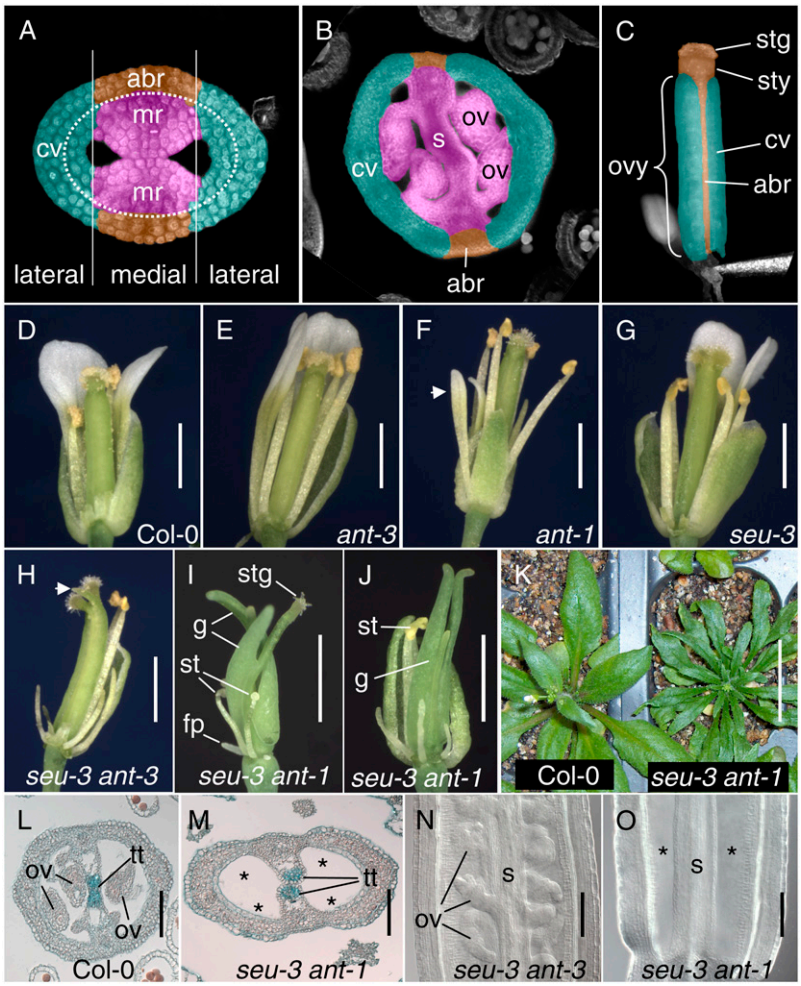

Figure 1. *seu ant* double mutants display enhanced vegetative, floral, and gynoecial phenotypes. A to C, False-colored photomicrographs. D to K, Photomicrographs of floral/rosette morphology; some sepals and petals have been removed from front half of flowers to allow viewing of gynoecium. L and M, Alcian-blue-stained gynoecial cross sections; N and O, Longitudinal optical section of cleared gynoecia (Nomarski optics). Scale bars: D to J, 1 mm; K, 10 mm; L to O, 0.1 mm. Asterisks (*) in M and O indicate expected location of ovules. A and B, Gynoecial cross sections at level of ovary from stage 8 (A) and stage 12 (B) flowers. Medial and lateral domains are shown subdivided into adaxial (inner) and abaxial (outer) portions by dotted oval. Two medial ridges (mr) arise on adaxial portions of medial domain (purple/magenta) at stage 8 and give rise to ovules (ov) and septum (s) in mature gynoecium. The abaxial replum (abr) forms from the abaxial portion of the medial domain (orange). The lateral domains gives rise to carpel valves (cv). C, Side view of mature gynoecium indicates patterning elements along apical basal axis: stigma (stg), style (sty), and ovary (ovy). D, Wild-type Col-0; E, *ant-3* mutant; F, *ant-1* mutant, petals narrower than wild type (arrowhead); G, *seu-3* mutant; H, *seu-3 ant-3* double mutant displays enhanced carpel splitting at apex (arrowhead); I and J, *seu-3 ant-1* double mutant displays filamentous petals (fp) and very reduced stamens (st); gynoecium (g) is split open and does not display ovules; medial domain displays small amounts of stigmatic (stg) and stylar tissue. K, Rosette phenotypes of Col-0 (left) and *seu-3 ant-1* (right). L, In Col-0 gynoecium transmitting tract (tt) stains blue and ovules (ov) are indicated. M, Transmitting tract stains blue in the *seu-3 ant-1* double mutant whereas ovules are missing. N, Developing ovules (ov) are observed attached to septum (s) in the *seu-3 ant-3* double mutant. O, In the *seu-3 ant-1* double mutant, no ovules grow out from septum (s).

protein families (Conner and Liu, 2000; van Meyel et al., 2003). Typically transcriptional coregulators do not interact directly with DNA, but rather regulate transcription by physically interacting with sequence-specific DNA-binding proteins (Courey and Jia, 2001; Matthews and Visvader, 2003). The *SEUSS* (*SEU*) gene shares a number of functional similarities to *LUG* during floral organ identity specification (Franks et al., 2002). *SEU* also encodes a transcriptional coregulator, albeit one with sequence similarity to the LIM-domain-binding protein family. SEU forms a transcriptional regulatory complex through a direct physical interaction with LUG that requires a functionally conserved LisH/LUFS domain found in LUG and the *Drosophila* protein Chip (van Meyel et al., 2003; Sridhar et al., 2004). The SEU/LUG protein complex is recruited to *AGAMOUS* (*AG*) regulatory sequences by the DNA-binding proteins SEPALLATA3 (SEP3) and APETALA1 (AP1) to repress *AG* in perianth organs (Sridhar et al., 2006).

Although *LUG*, *SEU*, and *ANT* all function in the repression of *AG* during floral development (Liu and Meyerowitz, 1995; Krizek et al., 2000; Franks et al., 2002) a number of experiments indicate that ectopic *AG* expression is not responsible for the loss of ovule primordia in the *lug ant* double mutant (Liu et al., 2000). These results suggest that *LUG*, *SEU*, and *ANT* direct the development of the gynoecium in part through the regulation of an *AG*-independent pathway(s). Data from petal development suggest that *SEU* and *LUG* are required for maintenance of the adaxial and abaxial polarity genes *PHABULOSA* (*PHB*) and *YABBY1/FILAMENTOUS FLOWER* (*YAB1/FIL*), respectively (Franks et al., 2006). In addition to its role in cellular proliferation, *ANT* also participates in organ polarity decisions (Nole-Wilson and Krizek, 2006). Together with *YAB1/FIL*, *ANT* is required for *PHB* expression in lateral organ primordia. These data taken together suggest that *SEU*, *LUG*, and *ANT* may regulate organ polarity and/or cellular proliferation during the development of the medial domain of the gynoecium.

Here we describe synergistic genetic interactions between *seu* and *ant* mutants. We detail the developmental abnormalities in *seu ant* double-mutant plants with a focus on patterning events during early gynoecial development. We demonstrate that *SEU* and *ANT*

provide two partially redundant, but parallel activities required for the development of the medial ridge and subsequent ovule initiation. Our results demonstrate that adaxial/inner identity is compromised early during the development of the gynoecium in *seu ant* mutants. We identify *PHB*, *REVOLUTA* (*REV*), and *CRABS CLAW* (*CRC*) as potential downstream targets of *SEU* and *ANT* regulation. In addition to the proposed linear regulatory relationship between *SEU* and the downstream targets *PHB*, *REV*, and *CRC*, our genetic analysis argues for an additional action of *SEU* in partially redundant pathway(s) parallel to *PHB*, *CRC*, and *ANT*.

RESULTS

seu ant Mutants Display Synergistic Floral and Vegetative Phenotypes

The *seu* single mutant has reduced stem length and shorter, rounder leaves (Franks et al., 2002). The *seu* plants also display multiple floral defects including partial homeotic transformations in perianth organs, narrower floral organs, reduction in stamen height and pollen production, partial splitting of the gynoecial apex, and ovule defects. Additionally, the *seu* plants display phenotypes associated with a decreased response to auxin, including decreased apical dominance, fewer lateral root primordia, and a reduced sensitivity to exogenous auxin (Pfluger and Zambryski, 2004). The *ant* single mutants display narrow floral organs, occasionally split carpel tips, ovule defects, slightly narrower leaves with reduced blade on the petiole section, and stamen locule defects (Elliott et al., 1996; Klucher et al., 1996).

To better understand the relationship of *SEU* and *ANT*, we generated *seuss aintegumenta* double-mutant plants. Organ counts in mature flowers revealed a synergistic role for *SEU* and *ANT* in the regulation of organ number in whorls 1 and 2 and in the control of organ size in all four whorls. The number of whorl-1 organs was significantly reduced in the *seu ant* double mutant, relative to wild type (Table I). Nearly all whorl-1 organs developed as narrow sepals (Fig. 2C), and no enhancement of homeotic transformation was detected. This is in contrast to whorl-1 organs in previously described *lug ant* flowers that typically display homeotic carpelloid transformations (Liu et al., 2000). The number of organs in whorl 2 was also significantly reduced in the *seu ant* mutant relative to wild type (Table I). In *seu-3 ant-1* mutants, whorl-2 organs developed as small radialized filamentous structures that failed to display cellular characteristics of mature petals (Fig. 1I; data not shown). Weaker allelic combinations employing the *ant-3* weak hypomorphic allele (Klucher et al., 1996) also displayed synergistic enhancement with respect to organ loss and organ shape and size (Fig. 1H). Scanning electron microscopy (SEM) analysis indicated that reduced numbers of floral organs resulted from early failure to initiate these organs (Fig. 2). In contrast to whorls 1 and 2, the effects of *seu* and *ant* on organ number in whorl 3 were additive (i.e. the number of stamens in the *seu-3 ant-1* double was similar to that in the *ant-1* single). Thus, most of the loss of stamens can be accounted for by the loss of *ANT* activity. The anthers of *ant* mutant stamens comprise just two locules compared to four locules in the wild-type anther (data not shown). The anther defect is further enhanced in the *seu-3 ant-1* mutant resulting in complete male sterility (Figs. 1, I and J, and 2, I and K). Carpel number was unchanged in all mutant combinations examined (Table I). However, the average length of mature stage-12 gynoecia (stages according to Smyth et al., 1990) from *seu-3 ant-1* mutants was statistically shorter than ecotype Columbia of Arabidopsis (Col-0) and either single mutant. The enhancement of carpel morphology observed in the *seu ant* double mutant is further described in the following section.

The rosette leaves of the *seu ant* mutants are shorter and narrower than those of either single mutant or

Table I. *Morphometric and phenotypic analysis of seu, ant, and seu ant mutant plants*

	Col-0	Col-*gl*	*ant-3*	*ant-1*	*seu-3*	*seu-3 ant-1*	*seu-3 ant-3*
Organ no. whorl 1	4.0 ± 0.0 $n = 20$	ND[a]	ND	3.9 ± 0.25 $n = 30$	4.0 ± 0.0 $n = 30$	2.6 ± 0.67[b] $n = 30$	ND
Organ no. whorl 2	4.0 ± 0.0 $n = 20$	ND	ND	3.97 ± 0.18 $n = 30$	4.0 ± 0.0 $n = 30$	2.9 ± 1.01[b] $n = 30$	ND
Organ no. whorl 3	5.9 ± 0.05 $n = 20$	ND	ND	4.2 ± 0.50[b] $n = 30$	5.6 ± 0.62 $n = 30$	3.7 ± 0.55[b] $n = 30$	ND
Organ no. whorl 4	2.0 ± 0.0 $n = 20$	ND	ND	2.0 ± 0.0 $n = 30$	2.0 ± 0.0 $n = 30$	2.0 ± 0.0 $n = 30$	ND
Average carpel length (in millimeters)	2.2 ± 0.12 $n = 10$	ND	ND	2.1 ± 0.17 $n = 9$	2.0 ± 0.19 $n = 10$	1.5 ± 0.22[b] $n = 10$	ND
Average ovules per carpel	25 ± 2.0 $n = 16$	21 ± 3.0 $n = 22$	20 ± 2.7 $n = 28$	12 ± 1.3[b] $n = 24$	23 ± 1.8 $n = 12$	0.0 ± 0.0[b] $n = 18$	13 ± 3.4[b] $n = 20$
Percent of ovules missing female gametophyte	0% $n = 76$	ND	13% $n = 30$	ND	22% $n = 106$	ND	76% $n = 45$

[a]ND, Not determined. [b]Indicates a statistically significant difference when compared to wild-type reference allele using Student's *t* test at $P < 0.001$.

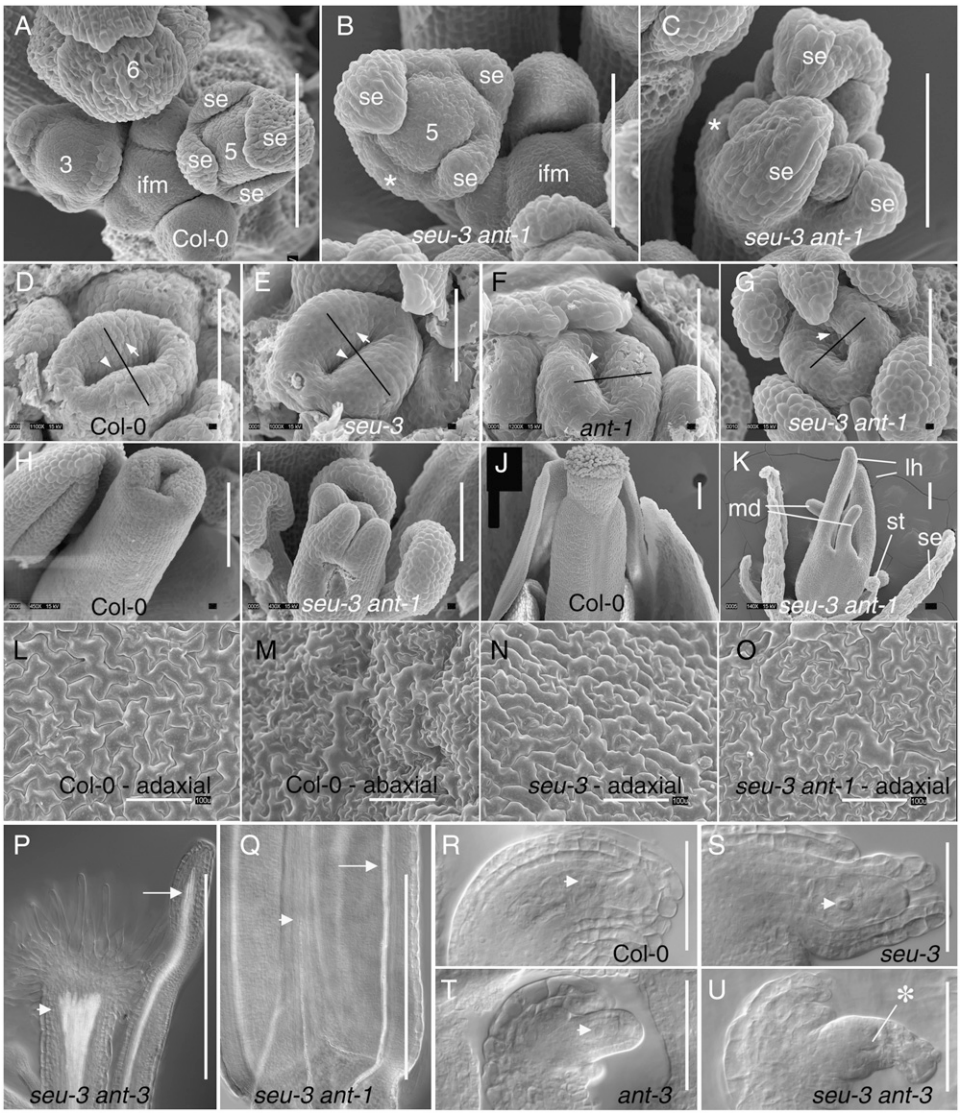

Figure 2. Early floral and ovule defects in *seu ant* double mutants. A to O, SEM micrographs. Numbers refer to stages of floral development. P to U, Nomarski contrast images of optically cleared tissue. Scale bars in A to C and H to O, 100 microns; bars in D to G and R to U, 50 microns; bars in P and Q, 500 microns. A, Col-0 inflorescence. Floral meristems display four sepals (se). Inflorescence meristem (ifm). B and C, *seu-3 ant-1* floral meristems display three narrow sepals. Locations of missing sepals indicated by asterisks (*). D to G, Stage-6 gynoecia of indicated genotypes. Black line indicates plane of medial domain. Arrowheads indicate medial ridges. Medial ridges appear reduced in G. H, Stage-11 Col-0 gynoecia. I, Stage-11 *seu-1 ant-3* gynoecium with enhanced apical splitting. J, Mature Col-0 gynoecium. K, Mature *seu-3 ant-1* flower. Gynoecium split at apex. Lateral carpel horns (lh) and medial domains (md) marked. Stamens (st) and sepals (se) reduced in size. L), Adaxial Col-0 leaf surface. M, Abaxial Col-0 leaf surface. N, Adaxial *seu-3* leaf surface. O, Adaxial *seu-3 ant-1* double-mutant leaf surface. Cells appear intermediate between adaxial and abaxial identities. P, Apex of *seu-3 ant-3* gynoecium. Vascular bundle in medial domain branches into stylar vascular array (arrowhead) similar to wild type. Lateral vascular bundle reaches apex (arrow). Q, Basal region of *seu-3 ant-1* gynoecium. Medial bundle terminates prematurely (arrowhead). Lateral bundle (arrow) reaches apex (not shown). R to U, Mature ovules of indicated genotypes. Arrowhead indicates central cell (R and S) or partially developed female gametophyte (T). The asterisk (*) in U indicates expected location of female gametophyte.

wild type (Fig. 1K). These shape changes are sometimes associated with a reduction in abaxial or adaxial fate assignment in the leaf (Waites and Hudson, 1995). To determine if the rosette leaves displayed adaxial or abaxial fate alterations, we examined epidermal cell morphology in the leaf blade by SEM. In wild-type rosette leaves, the leaf blade cells on both the adaxial and abaxial surfaces resemble jigsaw puzzle pieces. The cells of the adaxial surface are larger, more uniform in size, and less lobed than those of the abaxial surface (McConnell and Barton, 1998; Fig. 2, L and M). Additionally, the adaxial blade surface is flatter than

the abaxial blade surface; the later is more undulating. In *seu-3 ant-1* rosette leaves the adaxial leaf epidermal cells were slightly more lobed, more variable in size, and the leaf surface was more undulating when compared to wild type. These phenotypes suggest a partial loss of adaxial identity in *seu-3 ant-1* leaves (Fig. 2O). A similar but weaker effect was observed on the adaxial surface of the *seu-3* leaf (Fig. 2N). The edges of *seu-3* adaxial leaf cells appeared more lobed and the adaxial surface was more undulating compared to the flat adaxial surface of wild-type leaves. No alterations of epidermal cell morphology were observed on the abaxial leaf surfaces (data not shown). In addition to leaf defects, *seu ant* double mutants exhibited more severe internode elongation defects than either single mutant resulting in a semidwarf phenotype (data not shown).

seu ant Mutants Display Early Gynoecial Defects and Lack Ovule Primordia

To determine the effect of *seu* and *ant* on ovule initiation, we counted ovules from chloral hydrate-cleared stage-10 gynoecia. The average number of ovules observed in the *seu-3* single mutants was not statistically different from wild type (Table I). However, the *ant-1* single mutants averaged half the wild-type number of ovules. Notably, the *seu ant* double mutants lack ovules completely. Analysis of the double mutants by thin section analysis, SEM, and chloral hydrate clearing confirmed the complete loss of ovule primordia initiation (Figs. 1, L–O, and 2K). The *seu ant* double-mutant gynoecia, although split apart toward the apex, were fused normally in basal portions of the gynoecium. In these fused areas abaxial replum and some septal tissue formed (Fig. 1M). Alcian blue staining of cross sections was used to detect transmitting tract cells (Sessions and Zambryski, 1995). In Col-0, *ant-1*, and *seu-3* gynoecia, transmitting tract cells could be detected in all sections examined after stage 12 (Fig. 1L). In the *seu-3 ant-1* double mutants, transmitting tract cells could be detected in about 50% of the appropriately staged gynoecia (Fig. 1M). In many cases the extent of transmitting tract was reduced relative to the single mutants or wild type. In the other 50% of instances no transmitting tract was detected. Development of the stigmatic and stylar tissues was reduced in the *seu-3 ant-1* double mutant, but was detected (Fig. 1I). In comparison to the gynoecial phenotypes reported for the *lug ant* double mutant, the *seu ant* phenotypes are less severe. The *seu ant* gynoecia nearly always displayed stigma, style, and septum (albiet reduced), whereas *lug ant* gynoecia did not display stigmatic or stylar tissues, and only exhibited partial septum development when intermediate-strength *lug* alleles were examined (Liu et al., 2000). Furthermore, the degree carpel fusion is greater in the *seu ant* gynoecia, with component carpels nearly always fused together in the bottom third of the gynoecium, whereas the *lug ant* gynoecia are only infrequently fused to this degree. This is unlikely to be due to allele-specific or ecotype-specific effects because *seu-1 ant-9* double mutants in the L*er* ecotype display a phenotype that is similar to the *seu-3 ant-1* Col-0 ecotype plants reported here (R.G. Franks, unpublished data).

Weaker allelic combinations employing the *ant-3* hypomorphic allele (Klucher et al., 1996) also had synergistic ovule initiation defects. The average number of ovules in *ant-3* plants was not significantly different from the reference ecotype Col-*glabrous* (Col-*gl*; Table I). However, the *seu-3 ant-3* plants initiated significantly fewer ovules per carpel than either single mutant. The *seu-3 ant-3* double mutants also displayed enhanced splitting of the carpels (Fig. 1H). We examined mature, chloral hydrate-cleared *seu-3 ant-3* ovules and found no evidence of female gametophyte development in 76% of these ovules (Table I; Fig. 2, R–U). The other 24% of the *seu-3 ant-3* ovules displayed incompletely developed female gametophytes that appeared stalled at various stages of development. The *ant-3* and *seu-3* single-mutant ovules also displayed disrupted female gametophyte development, albeit less frequently than was observed in the double mutant (Table I). The extent of growth of the outer integument in *seu-3* and both the outer and inner integuments in *ant-3* was reduced relative to wild type (Fig. 2, R–U). This disruption of integument growth was more frequent and more pronounced in the *seu-3 ant-3* ovules than in the *seu-3* or *ant-3* single mutant. However, integument disruptions in the *seu-3 ant-3* ovules were less pronounced than in the strong loss-of-function *ant-1* single mutant that displays almost no integument development (Klucher et al., 1996).

We examined early stages of floral and gynoecial development in the *seu*, *ant*, and *seu ant* flowers with SEM to determine when morphological defects were first observed. The earliest morphological defect we observed in *seu ant* mutant floral meristems occurred at floral stage 3. In wild-type stage-3 flowers, four sepal primordia arise on the flanks of the floral meristem in whorl 1 (Fig. 2A). The *seu-3* and *ant-1* single mutants typically also displayed this morphology (data not shown). However in the *seu ant* double-mutant flowers, often only two or three sepal primordia were observed suggesting an early defect in organ initiation (Fig. 2, B and C).

Gynoecial development in wild-type flowers initiates at stage 6 as the gynoecial tube arises from the remaining portion of the floral meristem. In all genotypes we examined, including the *seu ant* double mutant, the gynoecial tube arose normally (Fig. 2, D–G). Shortly after the gynoecial tube forms, the medial ridges are observed as two distinct bulges on the adaxial (inner) surface of the tube in a medial position (Fig. 2D). These medial ridges will give rise to the placental tissue and ovule primordia, as well as septum and transmitting tract tissue. Development of gynoecia from *seu* or *ant* single-mutant flowers appears morphologically indistinguishable from wild type at this stage (Fig. 2, E and F). In some *seu ant*

gynoecia the early development of the medial ridge appears wild type. In other cases it appears to be reduced in its extent at this early stage of development, but still morphologically distinguishable (Fig. 2G). During stages 7 and 8, the gynoecial tube begins to elongate. In wild-type gynoecia, as well as in the *seu* and *ant* single mutants, this elongation is coordinated with respect to the medial and lateral domains ensuring a fused tube grows up evenly (Fig. 2H; data not shown). In the *seu ant* double mutants, splitting of the gynoecial apex results from the separation of the medial and lateral domains (Fig. 2I). Growth within the medial domains is retarded relative to the lateral domains and extended horn-like structures develop from the lateral domains in later stages (Fig. 2K).

In mature wild-type gynoecia the vascular bundles extend throughout the basal to apical extent of the ovary within the medial and the lateral domains (Kuusk et al., 2002). The lateral vascular bundle terminates at the distal portion of the ovary at the junction of the ovary and the style. The medial vascular bundle extends into the stylar tissue and terminates in a fan-shaped vascular array. Development of the medial and lateral vascular bundles was similar to wild type in the *seu-3 ant-3* double mutant (containing the hypomorphic *ant-3* allele; Fig. 2P, arrowhead). However, in the *seu-3 ant-1* double mutants, vasculature development in the two medial domains was retarded relative to that in wild-type and vascular bundles consistently terminated within the basal third of the gynoecium with no apparent development of the terminal vascular array (Fig. 2Q, arrowhead). The development of the lateral vascular bundles in the *seu-3 ant-1* double mutants was indistinguishable from wild type and terminated in the apex of the lateral horns (Fig. 2Q, arrow; data not shown).

seu ant Gynoecia Fail to Maintain Expression of Adaxial Fate Regulators *PHB* and *REV*

PHB, *PHAVOLUTA* (*PHV*), and *REV* are expressed within and are required for the specification of adaxial domains of Arabidopsis lateral organs (Zhong and Ye, 1999; Eshed et al., 2001; McConnell et al., 2001; Otsuga et al., 2001; Prigge et al., 2005). Additionally, they are expressed within adaxial portions of the gynoecium and are likely important for the specification of adaxial fate during gynoecium development (Otsuga et al., 2001; Prigge et al., 2005). As *SEU* and *ANT* regulate the expression of the polarity genes *YAB1/FIL* and *PHB* in petals and in leaves (Franks et al., 2006; Nole-Wilson and Krizek, 2006), we wondered if *SEU* and *ANT* regulate patterning events during gynoecial development. To test this we examined the expression of the adaxial patterning genes *PHB* and *REV* by in situ hybridization.

Within the wild-type floral meristem *PHB* is expressed within the adaxial core of the floral primordia from the preprimordium stage (anlagen) through stage 5 (Fig. 3, A and B; Prigge et al., 2005; Nole-Wilson and Krizek, 2006). At stage 5, the stamen primordia begin to separate from the future gynoecium (gynoecial anlagen), and *PHB* expression is detected in the core of the gynoecial anlagen as well as within the core region of the stamens (arrows); expression within the adaxial portions of the sepal is also detected (Fig. 3B). During stage 6, *PHB* expression continues to be detected within the core of the gynoecium and becomes more restricted within the stamen primordia to adaxial portions (Fig. 3, C and D). During stage 7, the expression domain in the gynoecial core resolves to two more lateral domains that likely mark the adaxial portions of the valve domains (Fig. 3E, arrowheads). Expression within the stamens is detected most strongly in an arc that may mark the boundary between adaxial and abaxial domains (Fig. 3E, arrow). The expression of *PHB* is strongest along this arc within marginal portions of the stamen. At later stages expression is detected in the placenta and early ovule primordia (Fig. 3F) and continues to be expressed in portions of the ovules (Sieber et al., 2004).

PHB expression within *seu* mutant flowers was indistinguishable from wild type at all stages examined (data not shown). Expression of *PHB* within *ant* mutant stage-3 flowers was detected in a pattern similar to that of stage-3 wild-type flowers (Fig. 3G). However, from stage 5 onward, the expression of *PHB* was weaker overall in the *ant* mutant flowers (Fig. 3, H–J). The reduced expression was more severe in the gynoecium than in the stamen primordia in which near wild-type levels of expression were typically detected (Fig. 3I, arrow). This molecular phenotype was not completely penetrant. However, we observed a loss or reduction of *PHB* signal during stages 5 or 6 in more than half of the *ant* mutant gynoecia examined. To control for variations in staining from experiment to experiment, we judged expression levels of *PHB* relative to expression levels in stage-3 flowers from the same in situ hybridization slide. In later stage gynoecia, stage 10 and older, *PHB* expression was strongly reduced or not detected in the *ant-1* gynoecium (Fig. 3J) although occasional exceptions with intermediate levels of staining were noted.

Within the *seu ant* double mutants, expression of *PHB* in stages 1 to 4 was indistinguishable from wild type (Fig. 3K). However, again we detected a reduction of expression within the adaxial core of the gynoecium at stages 5 and 6 that was more obvious in the *seu ant* double mutant than in the *ant* single mutant (compare Fig. 3L with Fig. 3D). This phenotype was also not fully penetrant at this stage, but was observed in more than half of the gynoecia examined. Expression of *PHB* was not detected in *seu ant* gynoecia older than stage 9 (Fig. 3M) except in vasculature tissues (data not shown). These results suggest that *SEU* and *ANT* play a role in the maintenance of expression of *PHB* expression during the transition of the floral meristem into the gynoecial primordia and at later stages of gynoecial development. These alterations in expression pattern, particularly those at stages 5 and 6,

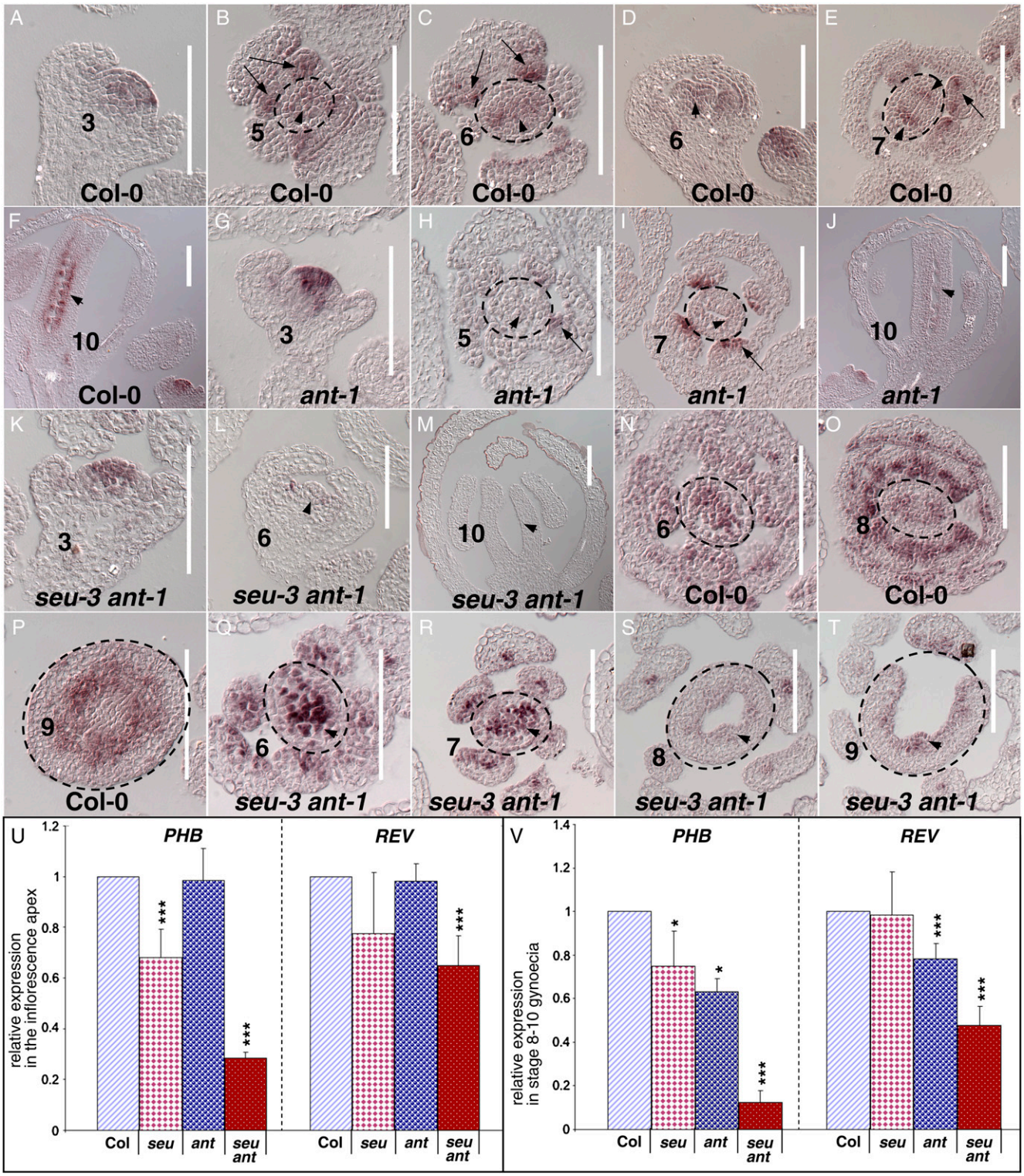

Figure 3. Adaxial fate determinants *PHB* and *REV* in *seu ant* gynoecia. In situ hybridization with *PHB* antisense (A–M) or *REV* antisense (N–T) probes. A, D, F, G, J, K, L, and M, Floral longitudinal sections. B, C, E, H, I, and N to T, Floral cross sections (extent of gynoecia encircled by black dashed ovals). All scale bars are 0.1 mm. Numbers refer to floral stages. A, *PHB* expression detected in central core of stage-3 Col-0 flower. B and C, *PHB* expression detected in adaxial core of gynoecial (arrowhead) and stamen (arrow) anlagen/primordia. D, *PHB* expression in gynoecium (arrowhead). E, *PHB* expression in adaxial valve domains of gynoecium (arrowheads). F, *PHB* expression in placenta and ovule primordia (arrowhead). G, *PHB* expression detected in central core of *ant-1* floral meristem. H and I, *PHB* expression is reduced or not detected in *ant-1* gynoecia (arrowheads). Expression in

preceded the earliest morphological alterations that are observed in *seu ant* gynoecia, suggesting that the loss of *PHB* expression is not simply due to a loss of the medial ridge precursors.

REV is also expressed within the adaxial core of early floral primordia, as well as the core of the gynoecial primordia (Otsuga et al., 2001; Prigge et al., 2005). *REV* continues to be expressed in adaxial portions of the gynoecium during stages 6 through 11 (Fig. 3, N–P). In *seu* and *ant* single mutants, expression of *REV* was indistinguishable from wild type (data not shown). In the *seu ant* double mutant, *REV* expression is strongly detected in the adaxial core of gynoecia (stages 6 and 7) at levels similar to wild type (Fig. 3, Q and R). By stages 8 and 9, expression within the adaxial gynoecium appeared reduced relative to wild type, however, weak expression was detected in adaxial portions of the gynoecium suggesting that adaxial fate is partially maintained in these double mutants (Fig. 3, S and T).

Quantitative real-time PCR (qRT-PCR) analysis confirmed the in situ hybridization studies. We examined expression levels from two different RNA sources: inflorescence apex (i.e. inflorescence meristem through floral stage 6) and dissected gynoecia from flowers (stages 8–10; Fig. 3, U and V). In the inflorescence apex, *PHB* levels in the *seu-3* and *seu-3 ant-1* genotypes were significantly reduced ($P < 0.001$) to 68% and 29% of wild-type levels, respectively. *REV* levels in the inflorescence apex were not significantly different from wild type in the *seu* or *ant* single mutants. In the *seu-3 ant-1* double mutant, *REV* levels did display a significant reduction compared to wild type. Consistent with our in situ hybridization data, the magnitude of this reduction was less than that observed for *PHB*. In the dissected gynoecia (stages 8–10), *PHB* levels in the *seu-3* and *ant-1* genotypes displayed a weakly significant ($P < 0.05$) reduction. The levels of *PHB* in the *seu ant* double-mutant gynoecia were further reduced to 12% of wild type ($P < 0.001$). Levels of *REV* in the dissected gynoecia also displayed highly significant reductions in the *ant-1* and *seu-3 ant-1* genotypes.

seu ant Gynoecia Display Altered Expression of Abaxial Fate Determinant *CRC*

The reduced levels of *PHB* and *REV* expression in the *seu ant* mutant suggest that adaxial identities may be compromised. Because of an antagonistic regulatory interaction between adaxial and abaxial fates in lateral organs, a reduction in adaxial fate is often accompanied by an ectopic expansion of abaxial fate (Bowman et al., 2002). To determine if abaxial fate was expanded in *seu ant* mutant carpels, we examined the expression of the gynoecial abaxial fate determinants *YAB1/FIL* and *CRC* by in situ hybridization. Both *CRC* and *YAB1/FIL* are members of the *YABBY* family of putative transcriptional regulators (Bowman and Smyth, 1999; Chen et al., 1999; Sawa et al., 1999; Siegfried et al., 1999). Genetic analysis indicates that *CRC* plays a role in the maintenance of abaxial fate in the medial domain of the carpel, a function that is partially redundant with *KANADI* and *GYMNOS* activities (Eshed et al., 1999).

In wild-type gynoecia *CRC* expression initiates during late stage 5 or early stage 6 within the abaxial valve domains (Fig. 4A; Bowman and Smyth, 1999). During late stage 7, expression is detected in a ring that includes the abaxial-most one or two cell layers of both the valve and margin domains (Fig. 4B, arrow). Expression in the abaxial epidermis continues in the margin domain through stage 10 and in the lateral domain into stage 11 (data not shown). During stage 7, *CRC* is also expressed within an internal expression domain that initiates as two stripes that appear to mark the boundary between the valve and margin domains (Fig. 4B, arrowheads; Bowman and Smyth, 1999). The internal expression domain may be important for ovule initiation or development (Bowman and Smyth, 1999; Alvarez and Smyth, 2002). During stage 8, the internal expression domain consists of the adaxial valve epidermal cell layer (Fig. 4C, asterisk) and four subepidermal foci (Fig. 4C, arrowheads) located close to the sites of ovule initiation. These foci span the boundary between the medial and lateral domains and consist of between 15 and 20 *CRC*-positive cells in an 8-micron tissue section. A slightly different pattern of *CRC* is detected in apical portions of the gynoecium (within 10–15 microns of the apex). In the gynoecial apex (stages 7 and 8), *CRC* is expressed throughout most of the of the valve domain, and in the abaxial medial domain, but is not expressed in the adaxial portions of the medial domain (i.e. the medial ridge; Fig. 4D).

The *seu* and *ant* single mutants display wild-type patterns of *CRC* expression (data not shown). However, alterations of *CRC* expression were observed in the *seu ant* double mutants. Expression in stage-6 *seu ant* gynoecia initiates normally (data not shown). However, in *seu ant* gynoecia (stages 7 and 8), *CRC* expression within internal domains was very reduced or absent whereas expression in the abaxial epidermis

Figure 3. (*Continued.*)
stamens is detected (arrows). J, *PHB* expression in placenta and ovule primordia (arrowhead) is reduced in *ant-1*. K, *PHB* expression is detected in stage-3 floral meristems of *seu ant* mutant. L and M, *PHB* expression is reduced in gynoecium (arrowheads). N to P, *REV* expression detected in the central portion of Col-0 gynoecium; stages 6 to 9. Q and R, *REV* expression detected in central portion of *seu ant* gynoecia (arrowheads). S and T, *REV* expression in gynoecia (stages 8 and 9) appears slightly reduced relative to wild type (compare S with O and T with P). U and V, qRT-PCR results. Relative expression levels for indicated genotypes from inflorescence apex (U) and stages 8 through 10 gynoecia (V). Statistically significant difference versus wild type; single asterisk (*), $P < 0.05$; triple asterisk (***), $P < 0.001$.

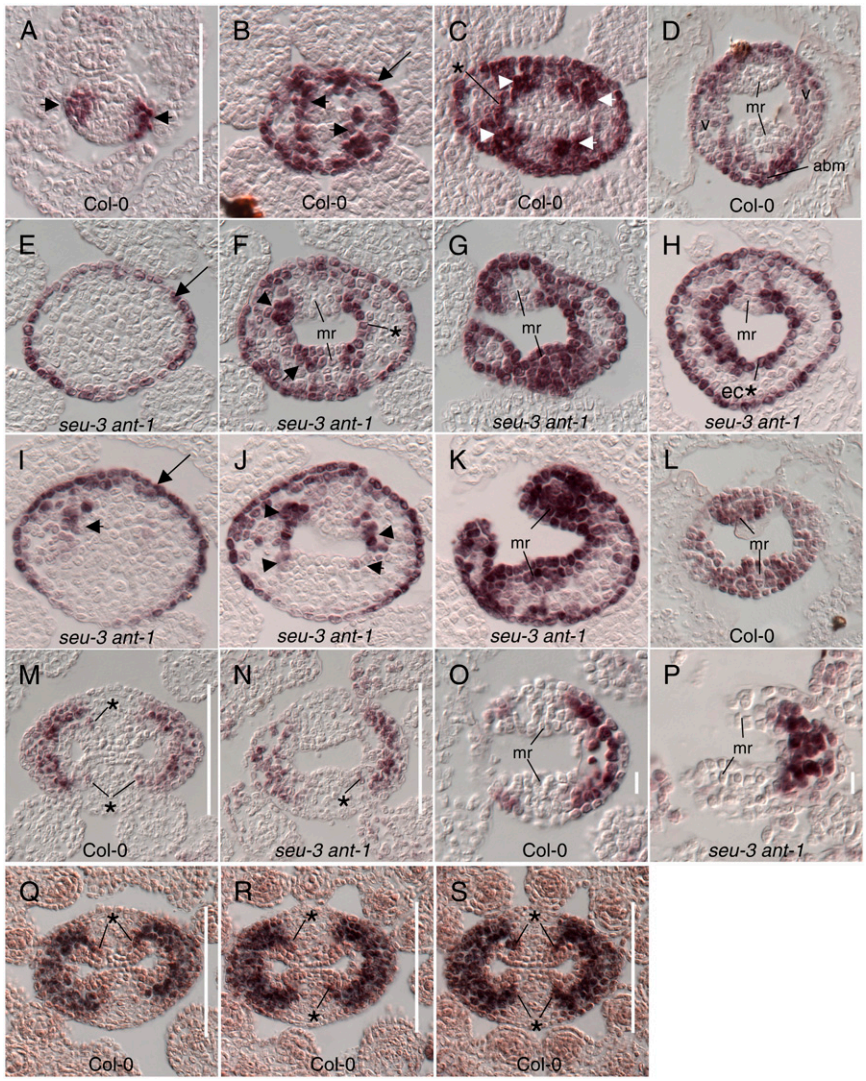

Figure 4. Abaxial fate determinants *YAB1/FIL* and *CRC* in *seu ant* gynoecia. In situ hybridization gynoecial cross sections. Probes in A to K, *CRC*; L, *ANT*; M to S, *YAB1/FIL*. A to L are at same scale. Scale bar in A, M to N, and Q to S, 0.1 mm; bar in O to P, 0.01 mm. A, Stage-6 wild-type section. Expression of *CRC* detected in two lateral valve domains (arrowheads). B, Expression of *CRC* at stage 7 observed in abaxial-most epidermal cells (arrow) and two internal stripes (arrowheads). C, Expression at stage 8 in abaxial epidermal cells, in four internal domains (arrowheads) and in adaxial valve epidermis (asterisk). D, Apical cross section, stage 8. *CRC* detected in valve domains (v) and more strongly in abaxial margin domains (abm), but is not detected in adaxial margin domains/medial ridge (mr). E to G, Serial gynoecial cross sections, each 24 microns apart. E, Basal section, *seu ant* gynoecium. *CRC* expression detected in abaxial epidermis, but no expression detected in internal domains. F, Midgynoecial section. *CRC* expression sometimes detected in internal domains, but domains are smaller and less consistently detected. Expression is detected in adaxial valve epidermis (asterisk). The lowermost of two medial ridges in this section appears reduced in size. G, Apical cross section. Ectopic expression of *CRC* detected in medial ridge (mr; compare to D). H, Midgynoecial section; only one of two medial ridges (mr) is detected. Ectopic epidermal (ec*) expression of *CRC* detected where medial ridge cells are expected. I to K, Serial gynoecial cross sections, each 24 microns apart. I, Basal cross section displays limited internal expression domains (arrowhead) while maintaining abaxial epidermal expression (arrow). J, Midgynoecial cross section. Limited expression in internal domains. K, Apical cross section. *CRC* ectopically detected in medial ridges. L, *ANT* expression in apical medial ridge (stage 8). M and N, Stage-9 cross sections of indicated genotypes. *YAB1/FIL* expression detected in abaxial valve mesophyl cells. Fingers of weaker expression (asterisk) extend into portions of medial domain that subtend ovules. These fingers are less consistently observed in the *seu ant* mutant (N). O and P, Stage-7 apical cross sections. *YAB1/FIL* expression is not detected in medial ridge (mr). Q, R, and S, Three serial cross sections (stage 8). Fingers of *YAB1/FIL* expression (asterisk) are often, but not always, detected subtending the sites of ovule initiation.

was still strongly detected. This was most clearly exhibited in the basal third of the gynoecium in which the internal expression domain was often not detected (Fig. 4E). At midgynoecial sections (Fig. 4F, H and J) expression of *CRC* in the internal expression domain was detected, but expression was weaker and disor-

ganized. The expression of *CRC* in the adaxial valve epidermis was more consistently detected than expression within the subepidermal foci. Typically from zero to five *CRC*-positive cells were detected in these foci in the *seu ant* mutant. Occasionally the extent of the medial ridge was reduced (Fig. 4F, bottom half of the gynoecium) or missing (Fig. 4H, bottom half of the gynoecium). In the apical portion of the *seu ant* gynoecium, we detected ectopic expression of *CRC* within the medial ridge. Although *CRC* is not normally expressed in the apical medial ridge in wild type (Fig. 4D), in the *seu ant* double mutants *CRC* was strongly detected in the medial ridge cells at the gynoecial apex (Fig. 4, G and K). These results indicate that *CRC* expression is differentially affected in the *seu ant* mutants along the apical/basal axis of the gynoecium. We note that *ANT* (Fig. 4L) and *SEU* (data not shown) are expressed in the medial domains at the apex of wild-type gynoecia and thus could be playing a direct role in the repression of *CRC* in these cells.

YAB1/FIL expression within the developing gynoecium is detected in abaxial subepidermal portions of the lateral domains that will later form the carpel valves (Fig 4M; Sawa et al., 1999; Siegfried et al., 1999). We also detected narrow rays or fingers of weaker expression that extend from the lateral domains into the portions of the medial domain that subtend the ovule primordia (Fig. 4, M, Q, R, and S). Serial cross sections indicated that these fingers were often, but not always, detected subtending sites of ovule primordium initiation. It appears that the cells of the *YAB1/FIL*-expressing fingers are a subset of the *CRC*-positive subepidermal foci cells, or closely abut them. *YAB1/FIL* expression in the *seu* and *ant* mutants appears to be unchanged relative to wild type. In the *seu ant* double-mutant *YAB1/FIL* is expressed normally in the abaxial valve domain, however, expression within the medial domain fingers was less consistently observed than in wild type (Fig. 4N). We also examined *YAB1/FIL* expression within the apex of the gynoecium. *YAB1/FIL* is not detected in the medial ridge at the gynoecial apex in wild-type gynoecia, nor in the *seu*, *ant* or *seu ant* mutants (Fig. 4, O and P). Thus, in contrast to *CRC*, *YAB1/FIL* is not ectopically expressed in the apical medial ridge in the *seu ant* double mutant.

SEU Protein Localizes to the Nucleus and Is Expressed Widely throughout the Plant

Northern analysis indicated that *SEU* RNA is expressed widely throughout all tissues examined (Franks et al., 2002). Examination of expression data available through the GENEVESTIGATOR site (Zimmermann et al., 2004) also suggest a widespread expression pattern for *SEU* RNA. *SEU* appears to play a role in determining expression of downstream target genes within domains of flower (repression of *AG* in perianth organs, but not reproductive structures; Franks et al., 2002; Sridhar et al., 2004, 2006) and domains of the gynoecium (this study). Thus, we wanted to examine the expression of the SEU protein during floral development to determine if localized expression of the SEU protein contributed to its specificity of action with respect to gene regulation. We generated C-terminal and N-terminal GFP translational fusion genomic rescue constructs: *pSEU::GFP:SEU* and *pSEU::SEU:GFP*. Three independent transformants were generated for each of the rescue constructs in a *seu-1* mutant background and all rescued the aboveground defects of the *seu-1* mutant (root phenotypes were not examined; data not shown). For all transformants, GFP florescence was detected in all tissues examined: root, young leaf, vegetative, and reproductive SAM, floral meristems, and all floral organs (Fig. 5; data not shown). GFP florescence was detected in the nucleoplasm, but was largely absent from the nucleolus and cytoplasm, or was detected at significantly reduced levels in these subcellular regions. Expression in the nucleoplasm is consistent with the predicted nuclear localization signal and the proposed role of SEU as a transcriptional coregulator (Franks et al., 2002). Within the developing

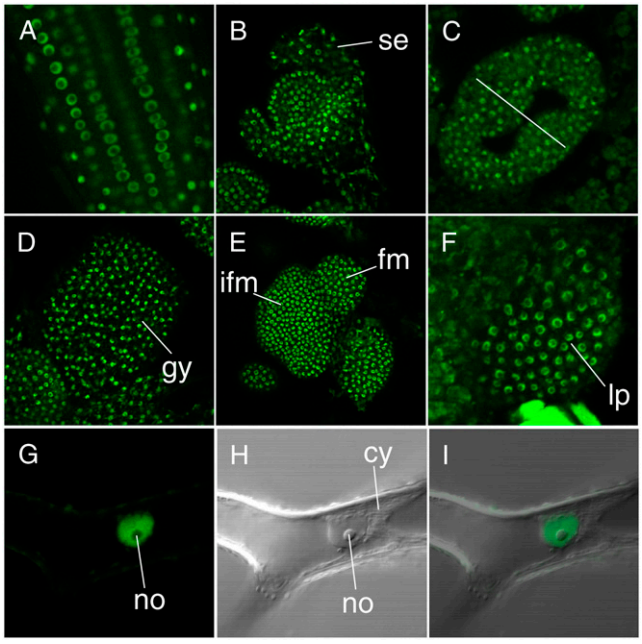

Figure 5. Expression of genomic SEUSS_GFP rescue construct. All images are from *seu-1* mutant plants phenotypically rescued by the pSEU::GFP:SEU fusion construct. A, pSEU::GFP:SEU expression in root division zone is detected in nearly all cells in the nucleus (nucleoplasm), but is not detected or is significantly reduced in the nucleolus and cytoplasm. B, Expression in the stage-3 floral bud optical longitudinal section is detected in all whorls; sepal (se). C, A stage-8 gynoecial optical cross section. Expression is detected throughout the gynoecium. Medial plane is indicated by line. Apparent cytoplasmic florescence is due to a difficulty imaging deep tissue layers and likely represents background florescence, not bona fide *GFP:SEU* expression. D, Stage-8 gynoecium (gy), optical longitudinal section. E, Inflorescence meristem (ifm) and young floral meristems (fm). F, Young rosette leaf primordium (lp). G to I, Trichome cell. G, GFP image. Expression is seen in nucleus, but not nucleolus (no), nor cytoplasm. H, Nomarski contrast image showing nucleolus (no) and cytoplasm (cy). I, Merged G and H.

floral meristem (Fig. 5B) and gynoecium (Fig. 5C), GFP fluorescence was detected throughout all stages and subdomains. The widespread expression of SEU protein indicates that localized expression of SEU is not responsible for its domain-specific action.

Genetic Interactions between *seu*, *crc*, and *ant*

Our in situ hybridization results indicate a complex relationship between *SEU*, *ANT*, and *CRC*. To better understand the regulatory relationships of these three genes, we analyzed *seu crc* double mutants and found that *seu* and *crc* displayed synergistic interactions with respect to carpel fusion and development of stigmatic tissues. In comparison to wild-type gynoecia, the *crc* mutant has a shorter and wider gynoecium that contains fewer ovules (Alvarez and Smyth, 1999, 2002; Fig. 6B). The *crc* gynoecium is also split within the apical-most third due to a failure of the two component carpels to maintain fusion. The *seu* single-mutant gynoecium often displays a small amount of splitting at the apex (Franks et al., 2002; Fig. 6C). This split is not between the two component carpels, but rather a split within the style or stigmatic tissue between the two fused marginal domains. The *seu crc* double-mutant gynoecium displays dramatically enhanced splitting between the two component carpels that extends for approximately 90% of the apical/basal extent of the gynoecium (Fig. 6D). The valves display horn-like extensions at the apex and there is an enhanced loss of stigmatic tissue. This synergistic enhancement between *seu* and *crc* is not found in *ant crc* double mutants that display a largely additive phenotype (Eshed et al., 1999; R.G. Franks, unpublished data).

Can the *seu ant* Double-Mutant Phenotype Be Rescued by Supplemental *PHB* Activity?

We sought to determine if the reduction of *PHB* expression in the *seu ant* double mutant was sufficient to explain the observed ovule loss. To test this, we attempted to rescue the *seu ant* carpel phenotype by replacing *PHB* expression with a *35S:PHB* construct. A *35S:PHB* expression construct (kindly provided by M. Prigge and S. Clark, University of Michigan, Ann Arbor, MI) that is functional to rescue the *phb phv cna athb8* mutant (Prigge et al., 2005) was crossed into the *seu ant* double mutant. Plants expressing the *35S:PHB* construct are wild type in appearance, are self-fertile, and display normal ovule initiation and development (McConnell et al., 2001; Prigge et al., 2005) likely due to the targeted degradation of *PHB* transcripts by microRNAs 165/166 in abaxial domains (Emery et al., 2003). In all observable phenotypes the *seu ant 35S:PHB/+* plants were indistinguishable from the *seu ant* double mutants (data not shown). These results indicate that the *35S:PHB* construct is not sufficient for rescue of the carpel defects of the *seu ant* mutant.

We additionally attempted to rescue the *seu ant* mutant with a *phb-1d* semidominant gain-of-function allele of *PHB* (McConnell and Barton, 1998; McConnell et al., 2001). To generate self-fertile *phb-1d* heterozygotes, plants were grown at 16°C (McConnell and Barton, 1998). The *phb-1d* allele generates a *PHB* transcript that is resistant to microRNA degradation and leads to the partial adaxialization of leaves, sepals, petals, and stamens (McConnell and Barton, 1998; McConnell et al., 2001; Emery et al., 2003). The *phb-1d/+* mutant gynoecium also displays signs of adaxialization including the growth of ectopic ovules (adaxial structures) from the abaxial base of the gynoecium (McConnell and Barton, 1998; McConnell et al., 2001). However, adaxially (within the *phb-1d/+* gynoecium) the initiation and development of ovules progresses normally, thus supporting female self-fertility. The presence of ovule primordia within the *phb-1d/+* gynoecium allowed us to test genetic epistasis of the *phb-1d* allele with respect to the ovule-less *seu ant* mutant phenotype. We reasoned that the *phb-1d* allele might replace lost adaxial activity in the *seu ant* mutant and thus rescue ovule development. We also reasoned that if

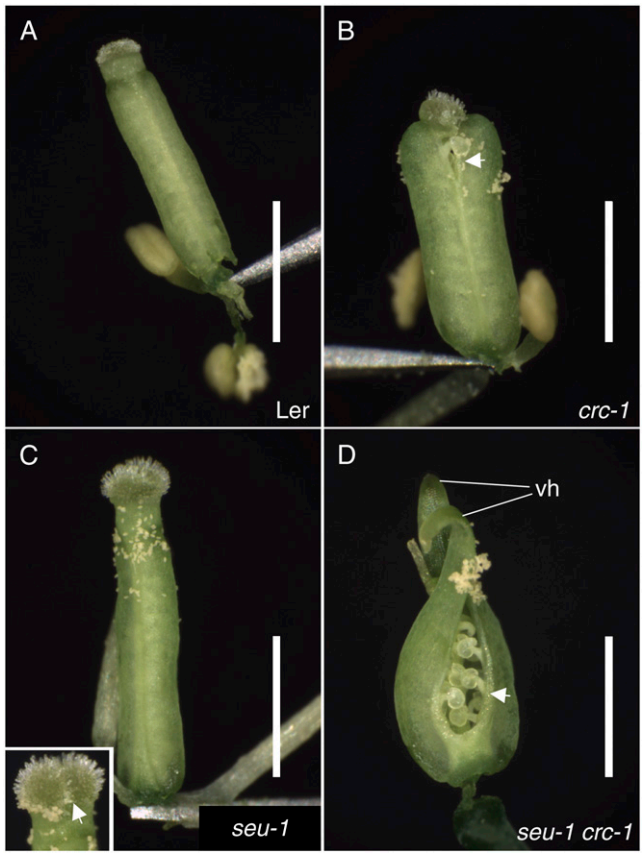

Figure 6. The *seuss crabs claw* double mutants display enhanced gynoecial defects. Photomicrographs of mature gynoecia of indicated genotypes. Scale bars are 1 mm for all panels. A, Landsberg *erecta* (L*er*) reference ecotype. B, Gynoecium of the *crabs claw* (*crc-1*) allele is shorter and wider than wild type with mild splitting at apex (arrowhead). C, Gynoecium of *seu-1* allele is slightly split at apex (arrowhead in inset). D, *seu-1 crc-1* double-mutant gynoecium displays enhanced splitting of carpels, exposing ovules (arrowhead). Valve horns (vh) are also exhibited.

SEU and *ANT* function upstream of *PHB* transcription that the loss of *SEU* and *ANT* might suppress or partially mitigate the *phb-1d* phenotype in the leaves and petals.

In the rosette leaves of the *phb-1d*/+ heterozygotes grown at 16°C, the area of the leaf blade is reduced and the petiole is longer relative to wild type (Fig. 7B). The rosette leaf phenotype of the *phb-1d/phb-1d* homozygote is more severe. These rosette leaves display only small amounts of laminar expansion of the leaf blade, and trumpet-shaped leaves were observed (Fig. 7D). In contrast to our expectations, we observed enhanced radialization and narrowing of rosette leaves in the *phb-1d/+ seu ant* mutants (Fig. 7C) approaching that exhibited by the *phb-1d* homozygote. We also observed an enhancement of the *phb-1d* homozygous phenotype in *phb-1d seu* double (Fig. 7E) and *phb-1d seu ant* mutants (Fig. 7F). Thus, the loss of *SEU*, or *SEU* and *ANT* together, caused a further radialization and loss of laminar expansion of rosette leaves in the *phb-1d* homozygote background. In these plants almost all leaves were completely radialized and rod shaped. These plants also did not produce an observable inflorescence whereas the *phb-1d* homozygotes did.

Floral phenotypes also indicated that the *seu* and *ant* mutations enhanced (in petals) or were epistatic to (in gynoecia) the *phb-1d* mutation, rather than functioning as suppressors. Enhancement in the degree of radialization was observed in the petals of *phb-1d/+ seu* and *phb-1d/+ ant* mutants relative to the *phb-1d/+* petals (Fig 7, J and K). With respect to the gynoecial phenotype, the *seu ant* double mutant was epistatic to the *phb-1d/+* mutant. The *phb-1d/+ seu ant* mutant gynoecia were very similar phenotypically to those of the *seu ant* double mutants in that medial domains formed but failed to generate ovule primordia (Fig. 7L).

DISCUSSION

ANT regulates organ initiation and organ size in part by maintaining the proliferative potential of organ primordia (Krizek, 1999; Mizukami and Fischer, 2000). More recent analysis of *ant fil* double mutants indicates that *ANT*, in concert with *YAB1/FIL*, is also involved in the regulation of floral organ identity and organ polarity along the abaxial/adaxial axis (Nole-Wilson and Krizek, 2006). *SEU* together with *LUG* has also been

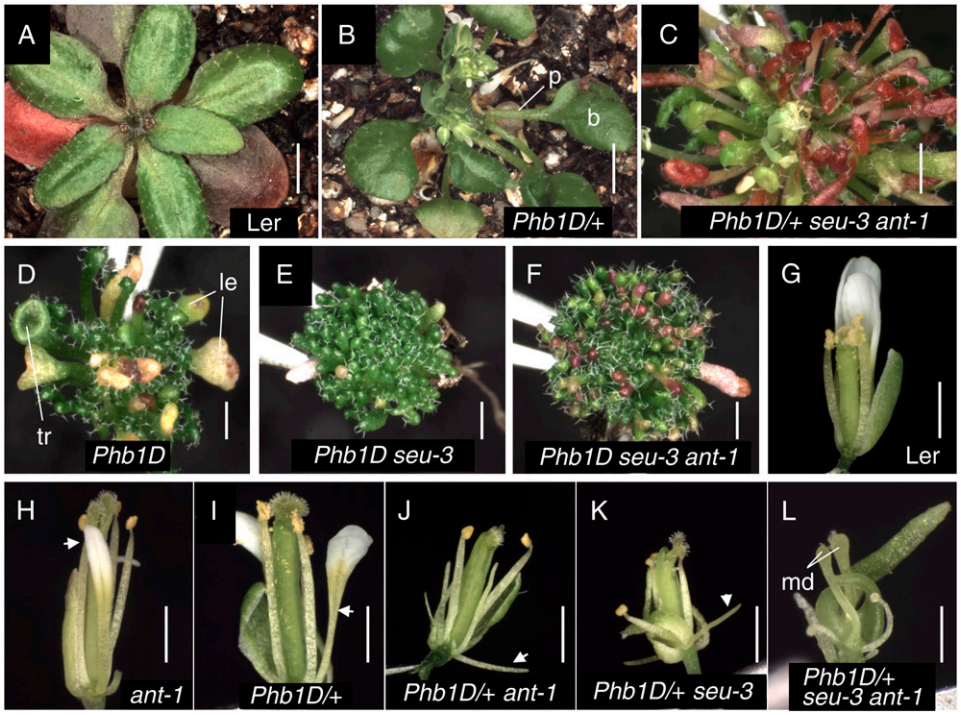

Figure 7. *SEU* and *ANT* function in parallel to *PHB*. A to F, Rosette phenotypes. G to L, Floral phenotypes of indicated genotypes. All plants grown at 16°C. Scale bars, A and B, 3 mm; C, 1.5 mm; D to K, 1 mm; and L, 0.5 mm. A, Wild-type Landsberg *erecta* (Ler). Primary bolt has been removed. B, *phb-1d*/+ plant. Rosette leaves display longer petiole (p) and smaller blade (b) than wild type. C, Rosette leaves of *phb-1d*/+ *seu-3 ant-1* are narrower and more strongly radialized than *phb-1d*/+ plants. D, *phb-1d* homozygous mutant. Rosette leaves display limited laminar expansion (le) and examples of trumpet (tr) shaped leaves. E, Rosette leaves of *phb-1d seu-3* display enhanced radialization and narrowing relative to *phb-1d* homozygote. F, Rosette leaves of *phb-1d seu-3 ant-1* triple mutant are similar to *phb-1d seu-3* double. G, Ler. H, *ant-1* displays narrow petals (arrowhead). I, *phb-1d*/+. Petals are slightly narrower, particularly in basal portion (arrowhead). J, *phb-1d*/+ *ant-1* displays filamentous petals (arrowhead). K, *phb-1d*/+ *seu-3* also displays filamentous petals. L, *phb-1d*/+ *seu-3 ant-1* is phenotypically similar to *seu-3 ant-1* double and displays severely split gynoecium. Margin domains (md) completely lack ovule primordia.

shown to regulate cell number during organogenesis, as well as organ identity and organ polarity (Franks et al., 2002, 2006). Here we report synergistic interactions between the *seu* and *ant* mutants in both vegetative and reproductive tissues. Our results indicate that *SEU* and *ANT* share a number of partially redundant functions during Arabidopsis development. The *seu ant* gynoecia display a complete loss of ovule initiation and a reduction of the gynoecial medial domain. These morphological defects may in part be due to a reduction in adaxial identity within the gynoecial core as well as a reduction of cell proliferation or growth within the medial domain. We identify *PHB*, *REV*, and *CRC* as potential downstream targets of *SEU* and *ANT* regulation in the gynoecium. Additionally, we propose that *SEU* is required to support the activities of genes that function in parallel to *ANT*, *PHB*, and *CRC* during the development of the medial domain of the gynoecium.

Expression of *PHB* and *REV* Are Reduced in the *seu ant* Gynoecium

SEU in concert with *LUG* has been shown to function in the maintenance of *PHB* expression in petals (Franks et al., 2006). *ANT* in concert with *YAB1/FIL* is required for the expression of *PHB* in leaves and developing flowers (Nole-Wilson and Krizek, 2006). Our data indicate that the accumulation of *PHB* RNA in the *seu ant* mutants is significantly reduced relative to wild type. This effect is most strongly observed in the adaxial core of developing gynoecium during stage 6 and in the adaxial valves during stages 7 through 10. The analysis of *REV* RNA accumulation indicates that *REV* RNA is also significantly reduced in the *seu ant* mutants. *REV* expression in early stages 6 and 7 appeared at wild-type levels by in situ hybridization whereas at later stages *REV* expression was slightly, but significantly reduced (Fig. 3). The detection of *REV* within the adaxial core of the gynoecium through stage 7 indicates that the reduction of *PHB* levels in the *seu ant* double are not simply due to a loss of cells in this zone of the gynoecium. Thus we propose that one action of *SEU* and *ANT* is to support the expression or accumulation of *PHB* and *REV* in the developing gynoecial core and thus potentiate adaxial identity within the gynoecium. Alvarez and Smyth (2002) propose a model in which the expression of adaxial identity genes within the adaxial valve domain is required for development of the placenta within the juxtaposed medial domain. Our data are consistent with this model. However, we report previously undocumented expression of *PHB* and *REV* within the adaxial portion of both the medial and lateral domains of the stage-6 gynoecium (Fig. 3). Thus, another interpretation is that placental specification and subsequent ovule initiation requires the expression of adaxial identity genes within the medial domain itself. The molecular identities of *SEU* and *ANT* as transcriptional regulators suggest that the regulation of *PHB* and *REV* RNA accumulation may be direct and at the transcriptional level, however, we cannot exclude other possibilities. A sequence that matches the ANT binding site consensus in 12 of 14 conserved positions (allowing for a single base-pair gap) is located 1,335 bp upstream of the *PHB* translation start site (data not shown). However, Nole-Wilson and Krizek (2006) failed to detect significant binding of a bacterial expressed ANT protein to this template in a gel shift assay.

We used two independent methods to replace *PHB* activity in the *seu ant* mutant to determine if adding back *PHB* could rescue the ovule-less phenotype. We found that neither a *35S:PHB* overexpression construct, nor the *phb-1d* allele provided rescue of the *seu ant* ovule loss (Fig. 7). These results suggest that the reduced expression of *PHB* is not likely sufficient, by itself, to explain loss of ovule primordia. *SEU* and *ANT* likely regulate additional genes during gynoecial development (e.g. *REV* and *CRC*) that may contribute to ovule initiation and medial domain development. An alternative, but not mutually exclusive, hypothesis is that *SEU* and *ANT* support cell division or growth within the medial domain independently from their role in the regulation of adaxial identity. The observation that *seu* and *ant* enhanced the leaf and petal defects of the *phb-1d* plants indicates a role of *SEU* and *ANT* in parallel to *PHB* in the regulation of laminar growth.

Expression of *CRC* Is Regulated in Different Directions by *SEU* and *ANT* in Apical versus Ovarian Portions of the Gynoecium

SEU and *ANT* together cooperate to regulate the expression of *CRC* within the developing gynoecium. However, the effect of *SEU* and *ANT* on *CRC* expression appears to be different in the apex of the gynoecium than it is in the ovary (Fig. 4). Within ovarian portions of the gynoecium, *SEU* and *ANT* support the expression of *CRC* in internal domains. However, within the apex of the gynoecium, *SEU* and *ANT* repress the expression of *CRC* in the medial ridge. Thus, the action of *SEU* and *ANT* on *CRC* expression likely depends on additional factors or may be indirect. In support of the former, SEU shares homology to the LIM-domain-binding protein family of transcriptional coregulators that have been shown to participate directly in both stimulatory and repressive transcriptional events in other systems by binding to a diversity of DNA-binding proteins (van Meyel et al., 2003). One speculation is that SEU and ANT mediate the action of an unidentified regulator of *CRC* expression that is differentially localized or active along the apical/basal axis of the gynoecium. Because a variety of experiments indicate that auxin signaling provides positional information along this axis (Sessions et al., 1997; Nemhauser et al., 2000; Balanza et al., 2006), it is possible that this proposed factor would be auxin dependent in some fashion.

The proximity of the *CRC* internal domain expression sites to the sites of ovule initiation, as well as a reduction in ovule initiation in *crc* mutants, suggest

that these internal domains may facilitate ovule initiation (Bowman and Smyth, 1999). The loss of the *CRC* internal domain expression in the *seu ant* gynoecia is consistent with these domains being important for ovule development. However, the presence of ovule formation, albeit reduced, in *crc* null alleles indicates that redundant activities for *CRC* likely exist. We show that small rays or fingers of *YAB1/FIL* expression extend into the medial domain and may overlap with the subepidermal foci expressing *CRC*. Given the sequence similarity between *YAB1/FIL* and *CRC*, it is possible that *YAB1/FIL* provides a partially redundant activity for ovule initiation.

The ectopic expression of *CRC* within the *seu ant* mutant indicates that *SEU* and *ANT* are required for the repression of *CRC* in the apical portion of the gynoecium. *LUG* has previously been shown to function as a negative regulator of *CRC* in perianth organs and a positive regulator of *CRC* in the internal gynoecium domains (Bowman and Smyth, 1999). In contrast to the ectopic *CRC* perianth expression reported for the *lug* mutant, we did not observe ectopic expression of *CRC* in the perianth organs of the *seu*, *ant*, or *seu ant* mutants (data not shown). We do not yet know the phenotypic significance of the ectopic *CRC* expression observed in the apical portions of the *seu ant* gynoecia. It is possible that this ectopic expression contributes to the apical defects of the *seu ant* mutant (enhanced loss of stigmatic and style tissues) or that misregulation of *CRC* at the apex contributes to the loss of ovules in the ovarian portions of the gynoecium. Further genetic analysis will be required to test these possibilities.

Differential Contributions of *SEU* and *LUG* to Gynoecial and Floral Development

The *seu ant* mutants fail to initiate ovule primordia and have reduced growth of other medial-ridge-derived tissues. Still the *seu ant* defect is less severe than the complete loss of the medial domain reported for the *lug ant* double (Liu et al., 2000). Thus *SEU* and *ANT* may regulate a subset of the genes regulated by *LUG* and *ANT* or may be less stringently required for the regulation of these genes. We note that in contrast to the *lug ant* mutant, the *seu ant* double mutants seldom display homeotic transformations of perianth organs and we did not observe ectopic expression of *AG* by in situ hybridization (data not shown). Thus, although SEU and LUG function as a molecular complex, SEU and LUG must make independent contributions to the activity of this complex and may be required to differing extents for the action of this complex during diverse regulatory interactions. The nonequivalence of SEU and LUG is further supported by the strong synergistic enhancement of floral phenotypes reported in the *seu lug* double mutants (Franks et al., 2002). One molecular explanation for a differential requirement for SEU and LUG is that they may have multiple protein partners and may participate in a number of different complexes that are required for diverse developmental events. A family of *SEUSS-LIKE* (*SLK*) genes has been described in Arabidopsis (Franks et al., 2002), and *Antirrhinum* members of this family have been shown to physically interact with *STYLOSA*, the *Antirrhinum LEU* ortholog (Navarro et al., 2004). Thus, the *SLK* gene family may support *SEU*-independent activities of *LUG* in the *seu* mutant plants.

SEU May Be Required for Functions That Are Redundant with *ANT* during Ovule Initiation and Medial Domain Development

ANT is expressed throughout the gynoecium in early stages and at highest levels in the adaxial core of the gynoecium before ovule initiation (Elliott et al., 1996). During ovule initiation and early ovule development *ANT* is strongly expressed in the medial ridge and the developing ovule primordia. Thus, *ANT* likely provides a key proliferative potential to the ovule primordia early in their development. In *ant* null allele mutants, however, ovule primordia initiate and continue to develop until the time of integument initiation indicating that *ANT* activity is not absolutely required for ovule initiation, per se (Elliott et al., 1996; Klucher et al., 1996). The complete loss of ovule initiation in the *seu ant* double suggests that *seu* may be required to potentiate the activity of *ANT*-independent pathways that provide a redundant proliferative or organ initiation activity during early ovule development. There are at least two pathways that might provide these redundant activities: *YABBY* genes and *AINTEGUMENTA-LIKE* (*AIL*) genes.

YABBY Gene Family

The observation that *fil ant* mutants display a near complete loss of the gynoecial medial domain demonstrates that *YAB1/FIL* provides an important function

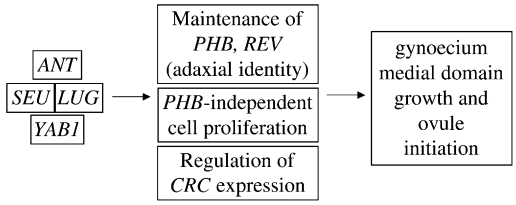

Figure 8. A model for the action of *SEU*, *LUG*, *ANT*, and *YAB1/FIL* in ovule initiation and gynoecium medial domain development SEU physically interacts with LUG to form a transcriptional coregulator complex. In wild-type plants the SEU/LUG coregulator complex works together with ANT and YAB1/FIL to regulate *PHB* and *REV* expression and maintain adaxial identity within the developing gynoecium. In parallel to the maintenance of *PHB* expression, the *SEU*, *LUG*, *ANT*, and *YAB1/FIL* activities stimulate cell proliferation in the developing gynoecium. *SEU*, *LUG*, and *ANT* also engender a position-dependent regulation of *CRC* expression: supporting *CRC* expression in the internal expression domains of the gynoecium and repressing *CRC* expression at the gynoecial apex. These three functions support ovule initiation and medial domain development in wild-type gynoecia.

that is partially redundant with *ANT* (Nole-Wilson and Krizek, 2006). The similar disruptions of medial domain development observed in the *seu ant* and *fil ant* double mutants suggest that *SEU* can potentiate the action of *ANT* in a manner similar to *YAB1/FIL*. The *fil ant* flowers also display a loss of floral meristem identity and floral organ identity that is characterized by reduced expression of *APETALA3* and ectopic *AG* expression. These phenotypes are not observed in the *seu ant* double mutants (data not shown), highlighting a degree of functional differentiation between SEU and YAB1/FIL. Evidence that *SEU* and *LUG* may physically cooperate with *YAB1/FIL* comes from the analysis of orthologous genes in *Antirrhinum majus* (Navarro et al., 2004). STYLOSA (STY), the *Antirrhinum* ortholog of LUG, has been shown to interact physically with members of the *Antirrhinum YABBY* and *SLK* gene families suggesting that the orthologous Arabidopsis proteins (SEU, YAB1/FIL, CRC, and LUG) may be part of a multimeric complex important for the development of the medial domain of the gynoecium.

Our report of a synergistic genetic interaction in the *seu crc* double mutant is the first report to our knowledge that demonstrates functional synergy between *seu* and a member of the *YABBY* gene family. Although our in situ hybridization results indicate that *SEU* and *ANT* work together to promote the expression of *CRC* within the internal expression domains, the genetic analysis of the *seu crc* double mutant suggests that *SEU* and *CRC* also function in partially redundant, parallel pathways with respect to carpel fusion and stigmatic tissue development.

AIL Gene Family

ANT is a member of a family of transcriptional regulators, the *AIL* gene family (Nole-Wilson et al., 2005). The expression of several members of the *AIL* family within the gynoecium overlaps with that of *ANT* suggesting that these genes may provide some functional redundancy. Interestingly, *ail6 ant* double mutants display a severe disruption of medial domain development that in some ways resembles that of the *fil ant*, *lug ant*, and *seu ant* double mutants (B. Krizek, unpublished data). One possibility is that *AIL6* provides functional redundancy in the *ant* mutant, where *SEU* is functional. However, in the *seu ant* mutant, *AIL6* activity may be compromised if its ability to function requires *SEU*.

A Model for Development of the Gynoecium Medial Domain

We propose a model for the action of *SEU*, *ANT*, and *LUG* during the development of the gynoecial medial domain (Fig. 8). We speculate that the SEU/LUG coregulator complex physically interacts with YAB1 and/or ANT. This multimeric complex can: (1) potentiate the expression of the adaxial fate determinants (*PHB* and *REV*) in the adaxial core of stages 6 to 8 developing carpel; (2) support cellular proliferation within the medial ridge and the initiating ovule primordia through a *PHB*-independent pathway; and (3) engender a position-dependent regulation of *CRC* expression, supporting *CRC* expression in the internal expression domains of the gynoecium and repressing *CRC* expression at the gynoecial apex. These three functions support medial domain development and ovule initiation in wild-type gynoecia. Additional members of the *SLK* (Franks et al., 2002; Navarro et al., 2004), *AIL* (Nole-Wilson et al., 2005), *YABBY* (Siegfried et al., 1999), and *LUG/LEUNIG-HOMOLOGUE* (Conner and Liu, 2000) gene families are likely to provide molecular redundancy by also participating in this multicomponent molecular complex. Mutant combinations that disrupt at least two of these protein subunits can result in a dramatic loss of the gynoecium medial domain (e.g. *lug ant*, *fil ant*, and *ail6 ant*; Liu et al., 2000; Nole-Wilson and Krizek, 2006; B. Krizek, unpublished data), a loss of ovules from the medial domain (e.g. *seu ant*; this study), or a near complete deletion of the entire gynoecium (e.g. *seu lug*; Franks et al., 2002).

MATERIALS AND METHODS

In Situ Hybridization

In situ hybridizations were carried out as previously reported (Franks et al., 2002). A detailed in situ hybridization protocol is available at http://www4.ncsu.edu/~rgfranks/protocols.html. In situ hybridization probes were in vitro transcribed from the following plasmids: *ANT*, p5delta4; *CRC*, pCRII_CRCc1; *PHB*, pPHB-AS (gift of J. Bowman, Monash University, Victoria, Australia); *REV*, pCRII_REVc4; *YAB1/FIL*, pY1-Y (gift of J. Bowman).

Microscopy

SEM was carried out as previously reported (Franks et al., 2006) except that the images were collected on a JEOL 5900LV. Chloral hydrate clearing (Berleth and Jurgens, 1993) and Alcian blue staining (Sessions and Zambryski, 1995) were performed as described. In situ, Nomarski, and Alcian-blue-stained samples were imaged on an Axioscop2 microscope (Zeiss) and captured with a MicroPublisher 5.0 RTV digital camera and QCapture software (QImaging). Stereoscope images were collected with the same camera on a MX12.5 stereoscope (Leica). Confocal images were collected on a IMBE inverted confocal microscope (Leica) at standard GFP settings.

Tissue Dissection, RNA Extraction, and qRT-PCR

Whole inflorescences were collected in 100% ice cold ethanol, fixed overnight at 4°C, and then dissected under a MX12.5 stereomicroscope (Leica) while submersed in 100% ethanol. Tissue was stored in 100% ethanol at 4°C or −20°C for up to 1 week while appropriate development stages were dissected. Ethanol was removed and tissue frozen in liquid nitrogen and then ground. RNA extraction was performed using TRI reagent (Molecular Research Center) according to manufacturer's instructions. The cDNA synthesis was performed using the SuperScript first-strand synthesis system for qRT-PCR (Invitrogen) with a oligo(dT)-primer, according to the manufacturer's instructions. The qRT-PCR was performed on an ABI 7900 using the QuantiTect SYBR Green PCR kit (QIAGEN). In a single PCR run, all samples were done in triplicate, averaged, and normalized using the levels of *ADENOSINE PHOSPHORIBOSYL TRANSFERASE* gene (*APT*; At1g27450); *APT* expression levels of the parental ecotype (Col) were set to a relative level of 1.0. Expression levels of *PHB* and *REV* were displayed as a fraction of the wild-type (Col) value. Dissociation curve analysis was performed at the end of each run to

ensure the specificity of each reaction. Figure 3, U and V, shows the average relative expression of six PCR runs (three from each of two biological replicates). A Student's *t* test for significance was performed on these six normalized averages. Primers used for qRT-PCR analysis are as follows: for *APT*, RTAPT-3 and RTAPT-4; for *PHB*, RTPHB-1 and RTPHB-2; for *REV*, RTREV-1 and RTREV-2. Sequences of these primers are reported in the supplemental data.

Genetic Analysis and Plant Growth

All of the alleles used in this study have been previously described: *ant-1* and *ant-3* (Klucher et al., 1996) were backcrossed into Col-0 three and seven times, respectively, before our genetics analysis; *ant-9* (Elliott et al., 1996); *crc-1* (Alvarez and Smyth, 1999); *phb-1d* (McConnell and Barton, 1998); *seu-1* (Franks et al., 2002); *seu-3* (Pfluger and Zambryski, 2004). All genotypes were confirmed by PCR-based markers. Details for these markers are provided in the supplemental data. Plants were grown in growth chambers at 22°C to 24° C with a 16-h/8-h photoperiod under fluorescent light at 80 to 150 μmol m^{-2} s^{-1}.

Generation of *seu ant 35S:PHB* Plants

Seeds containing the *35S:PHB* construct in a *phb-12 phv-11 cna-2 athb8-12* quadruple mutant background were obtained from Dr. Steven Clark (Prigge et al., 2005). *35S:PHB phb-12 phv-11 cna-2 athb8-12* plants were crossed to *seu-3*. F_1 progeny were then crossed to *ant-1*. F_2 progeny segregating both the *seu-3* and *ant-1* alleles were verified by PCR genotyping. This and subsequent generations were used for phenotype analysis. At each step, plants containing the *35S::PHB* transgene were identified by selection on plates containing Basta prior to growth in soil. Loss of the original quadruple mutant background was also verified by PCR genotyping as previously described (Prigge et al., 2005).

Generation of *phb-1d/+ seu-3 ant-1* Plants

phb-1d/+ (heterozygous) seeds were obtained from the Arabidopsis Biological Resource Center (stock CS3761) and grown at 16°C. *phb-1d/+* plants were crossed to *ant-1*. F_1 progeny with a *phb-1d/+ ant-1/+* genotype were then crossed to *seu-3*. *phb-1d/+ seu-3 ant-1* plants from the F_2 and subsequent generations were used for phenotype analysis. All genotypes were confirmed by PCR-based markers. Details for these markers are provided in the supplemental data.

pSEU::SEU:GFP and *pSEU::GFP:SEU* Constructs

For details of the construction of *pSEU::SEU:GFP* and *pSEU::GFP:SEU* constructs, see the supplemental data. Three independent transformant lines for both pSEU::SEU:GFP and pSEU::GFP:SEU were obtained by the simplified *Argobacterium* floral dip method (Clough and Bent, 1998). All six of these lines rescued all of the aboveground *seu-1* mutant phenotypes (data not shown). Expression from these six transformant lines was consistent between the individual lines. Transformant plants were examined in the T_2 and T_3 generations.

Supplemental Data

The following materials are available in the online version of this article.

Supplemental Figure S1. Details of construction of *pSEU::SEU:GFP* and *pSEU::GFP:SEU*.

Supplemental Figure S2. Genotyping for mutant alleles used in this study.

Supplemental Table S1. Oligonucleotides used in this study.

ACKNOWLEDGMENTS

We thank Z. Liu and R. Fischer for support of this project from its inception; J. Pfluger, G. Drews, and C. Grossinger for technical advice; M. Prigge, S. Clark, and J. Bowman for sharing reagents and seeds; B. Krizek for sharing unpublished results; Z. Liu, J. Reed, J. Mahaffey, and anonymous reviewers for helpful comments on the manuscript; the Arabidopsis Biological Resource Center for distribution of seeds; and the North Carolina State University Center for Electron Microscopy and Cellular and Molecular Imaging Facility.

Received December 11, 2007; accepted January 2, 2008; published January 9, 2008.

LITERATURE CITED

Alvarez J, Smyth DR (1999) *CRABS CLAW* and *SPATULA*, two *Arabidopsis* genes that control carpel development in parallel with *AGAMOUS*. Development **126:** 2377–2386

Alvarez J, Smyth DR (2002) *CRABS CLAW* and *SPATULA* genes regulate growth and pattern formation during gynoecium development in *Arabidopsis thaliana*. Int J Plant Sci **163:** 17–41

Balanza V, Navarrete M, Trigueros M, Ferrandiz C (2006) Patterning the female side of Arabidopsis: the importance of hormones. J Exp Bot **57:** 3457–3469

Berleth T, Jurgens G (1993) The role of *monopteros* in organizing the basal body region of the *Arabidopsis* embryo. Development **118:** 575–587

Bowman JL, Baum SF, Eshed Y, Putterill J, Alvarez J (1999) Molecular genetics of gynoecium development in *Arabidopsis*. Curr Top Dev Biol **45:** 155–205

Bowman JL, Eshed Y, Baum SF (2002) Establishment of polarity in angiosperm lateral organs. Trends Genet **18:** 134–141

Bowman JL, Smyth DR (1999) *CRABS CLAW*, a gene that regulates carpel and nectary development in *Arabidopsis*, encodes a novel protein with zinc finger and helix-loop-helix domains. Development **126:** 2387–2396

Chen Q, Atkinson A, Otsuga D, Christensen T, Reynolds L, Drews GN (1999) The Arabidopsis FILAMENTOUS FLOWER gene is required for flower formation. Development **126:** 2715–2726

Clough SJ, Bent AF (1998) Floral dip: a simplified method for Agrobacterium-mediated transformation of Arabidopsis thaliana. The Plant Journal **16:** 735–743

Conner J, Liu Z (2000) *LEUNIG*, a putative transcriptional corepressor that regulates *AGAMOUS* expression during flower development. Proc Natl Acad Sci USA **97:** 12902–12907

Courey AJ, Jia S (2001) Transcriptional repression: the long and the short of it. Genes Dev **15:** 2786–2796

Elliott RC, Betzner AS, Huttner E, Oakes MP, Tucker WQ, Gerentes D, Perez P, Smyth DR (1996) *AINTEGUMENTA*, an *APETALA2*-like gene of *Arabidopsis* with pleiotropic roles in ovule development and floral organ growth. Plant Cell **8:** 155–168

Emery JF, Floyd SK, Alvarez J, Eshed Y, Hawker NP, Izhaki A, Baum SF, Bowman JL (2003) Radial patterning of *Arabidopsis* shoots by class III HD-ZIP and *KANADI* genes. Curr Biol **13:** 1768–1774

Eshed Y, Baum SF, Bowman JL (1999) Distinct mechanisms promote polarity establishment in carpels of *Arabidopsis*. Cell **99:** 199–209

Eshed Y, Baum SF, Perea JV, Bowman JL (2001) Establishment of polarity in lateral organs of plants. Curr Biol **11:** 1251–1260

Ferrandiz C, Pelaz S, Yanofsky MF (1999) Control of carpel and fruit development in Arabidopsis. Annu Rev Biochem **68:** 321–354

Franks RG, Liu Z, Fischer RL (2006) SEUSS and LEUNIG regulate cell proliferation, vascular development and organ polarity in Arabidopsis petals. Planta **224:** 801–811

Franks RG, Wang C, Levin JZ, Liu Z (2002) *SEUSS*, a member of a novel family of plant regulatory proteins, represses floral homeotic gene expression with *LEUNIG*. Development **129:** 253–263

Klucher KM, Chow H, Reiser L, Fischer RL (1996) The *AINTEGUMENTA* gene of *Arabidopsis* required for ovule and female gametophyte development is related to the floral homeotic gene *APETALA2*. Plant Cell **8:** 137–153

Krizek BA (1999) Ectopic expression of *AINTEGUMENTA* in *Arabidopsis* plants results in increased growth of floral organs. Dev Genet **25:** 224–236

Krizek BA, Prost V, Macias A (2000) *AINTEGUMENTA* promotes petal identity and acts as a negative regulator of *AGAMOUS*. Plant Cell **12:** 1357–1366

Kuusk S, Sohlberg JJ, Long JA, Fridborg I, Sundberg E (2002) STY1 and STY2 promote the formation of apical tissues during Arabidopsis gynoecium development. Development **129:** 4707–4717

Liu Z, Franks RG, Klink VP (2000) Regulation of gynoecium marginal tissue formation by *LEUNIG* and *AINTEGUMENTA*. Plant Cell **12:** 1879–1892

Liu Z, Meyerowitz EM (1995) *LEUNIG* regulates *AGAMOUS* expression in *Arabidopsis* flowers. Development **121:** 975–991

Matthews JM, Visvader JE (2003) LIM-domain-binding protein 1: a multifunctional cofactor that interacts with diverse proteins. EMBO Rep **4:** 1132–1137

McConnell JR, Barton MK (1998) Leaf polarity and meristem formation in *Arabidopsis*. Development **125:** 2935–2942

McConnell JR, Emery J, Eshed Y, Bao N, Bowman J, Barton MK (2001) Role of *PHABULOSA* and *PHAVOLUTA* in determining radial patterning in shoots. Nature **411:** 709–713

Mizukami Y, Fischer RL (2000) Plant organ size control: *AINTEGUMENTA* regulates growth and cell numbers during organogenesis. Proc Natl Acad Sci USA **97:** 942–947

Navarro C, Efremova N, Golz JF, Rubiera R, Kuckenberg M, Castillo R, Tietz O, Saedler H, Schwarz-Sommer Z (2004) Molecular and genetic interactions between STYLOSA and GRAMINIFOLIA in the control of Antirrhinum vegetative and reproductive development. Development **131:** 3649–3659

Nemhauser JL, Feldman LJ, Zambryski PC (2000) Auxin and *ETTIN* in Arabidopsis gynoecium morphogenesis. Development **127:** 3877–3888

Nole-Wilson S, Krizek BA (2000) DNA binding properties of the Arabidopsis floral development protein AINTEGUMENTA. Nucleic Acids Res **28:** 4076–4082

Nole-Wilson S, Krizek BA (2006) *AINTEGUMENTA* contributes to organ polarity and regulates growth of lateral organs in combination with *YABBY* genes. Plant Physiol **141:** 977–987

Nole-Wilson S, Tranby TL, Krizek BA (2005) AINTEGUMENTA-like (AIL) genes are expressed in young tissues and may specify meristematic or division-competent states. Plant Mol Biol **57:** 613–628

Otsuga D, DeGuzman B, Prigge MJ, Drews GN, Clark SE (2001) *REVOLUTA* regulates meristem initiation at lateral positions. Plant J **25:** 223–236

Pfluger J, Zambryski P (2004) The role of SEUSS in auxin response and floral organ patterning. Development **131:** 4697–4707

Prigge MJ, Otsuga D, Alonso JM, Ecker JR, Drews GN, Clark SE (2005) Class III homeodomain-leucine zipper gene family members have overlapping, antagonistic, and distinct roles in *Arabidopsis* development. Plant Cell **17:** 61–76

Sawa S, Watanabe K, Goto K, Kanaya E, Morita EH, Okada K (1999) FILAMENTOUS FLOWER, a meristem and organ identity gene of Arabidopsis, encodes a protein with a zinc finger and HMG-related domains. Genes Dev **13:** 1079–1088

Sessions A (1999) Piecing together the Arabidopsis gynoecium. Trends Plant Sci **4:** 296–297

Sessions A, Nemhauser JL, McColl A, Roe JL, Feldmann KA, Zambryski PC (1997) *ETTIN* patterns the *Arabidopsis* floral meristem and reproductive organs. Development **124:** 4481–4491

Sessions RA, Zambryski PC (1995) *Arabidopsis* gynoecium structure in the wild and in *ettin* mutants. Development **121:** 1519–1532

Sieber P, Gheyselinck J, Gross-Hardt R, Laux T, Grossniklaus U, Schneitz K (2004) Pattern formation during early ovule development in Arabidopsis thaliana. Dev Biol **273:** 321–334

Siegfried KR, Eshed Y, Baum SF, Otsuga D, Drews GN, Bowman JL (1999) Members of the *YABBY* gene family specify abaxial cell fate in *Arabidopsis*. Development **126:** 4117–4128

Smyth DR, Bowman JL, Meyerowitz EM (1990) Early flower development in *Arabidopsis*. Plant Cell **2:** 755–767

Sridhar VV, Surendrarao A, Gonzalez D, Conlan RS, Liu Z (2004) Transcriptional repression of target genes by LEUNIG and SEUSS, two interacting regulatory proteins for Arabidopsis flower development. Proc Natl Acad Sci USA **101:** 11494–11499

Sridhar VV, Surendrarao A, Liu Z (2006) APETALA1 and SEPALLATA3 interact with SEUSS to mediate transcription repression during flower development. Development **133:** 3159–3166

van Meyel DJ, Thomas JB, Agulnick AD (2003) Ssdp proteins bind to LIM-interacting co-factors and regulate the activity of LIM-homeodomain protein complexes *in vivo*. Development **130:** 1915–1925

Waites R, Hudson A (1995) *phantastica*: a gene required for dorsoventrality of leaves in *Antirrhinum majus*. Development **121:** 2143–2154

Zhong R, Ye ZH (1999) IFL1, a gene regulating interfascicular fiber differentiation in Arabidopsis, encodes a homeodomain-leucine zipper protein. Plant Cell **11:** 2139–2152

Zimmermann P, Hirsch-Hoffmann M, Hennig L, Gruissem W (2004) GENEVESTIGATOR. Arabidopsis microarray database and analysis toolbox. Plant Physiol **136:** 2621–2632